Dynamics of Torsional Vibration Damper (TVD) pulley, implementation of a rubber elastomeric behavior, simulations and experiments

C.A.F. Silva, Lionel Manin, R.G. Rinaldi, Etienne Besnier, Didier Remond

Dynamics of Torsional Vibration Damper (TVD) pulley, implementation of a rubber elastomeric behavior, simulations and experiments

C. A. F. Silva[1], L. Manin[1*], R. G. Rinaldi[2], E. Besnier[1], D. Remond[1]

[1] Univ Lyon, INSA-Lyon, CNRS UMR5259, LaMCoS, F-69621, Villeurbanne France

[2] Univ Lyon, INSA-Lyon, CNRS UMR5521, Mateis, F-69621, Villeurbanne, France

* Corresponding author e-mail address: lionel.manin@insa-lyon.fr

Abstract

In this work, the Torsional Vibration Damper (TVD) rubber ring viscoelastic-material properties are determined based on Dynamical Mechanical Analysis (DMA) measurements and master curves reconstructions using thermo-simplicity principle. The elastomeric constitutive behavior is then implemented in the torsional vibration damper's equation of motion and the frequency response is simulated so that enhanced physical representation of the TVD dynamics can be achieved. Major differences in the TVD frequency response are highlighted and analyzed whether or not the viscoelastic material properties (elasticity modulus and damping) are considered constant or frequency and temperature dependent.

1 Introduction

The Torsional Vibration Damper (TVD) is an essential component of power transmission systems such as the Front Engine Accessory Drives (FEAD). The FEAD of a vehicle is a system composed of individual accessories such as compressor, alternator, water and steering pumps, etc. These accessories are coupled to pulleys which are driven in rotation by a poly-V belt driven itself by the crankshaft pulley (Fig.1). This driving pulley is commonly used as a torsional vibration damper for the crankshaft since rotational vibrations are harmful to the system performance and may cause fatigue. The TVD is usually tuned so that to dampen the first torsional mode of the crankshaft and therefore provide rotational speed stability. The pulley (outer ring) is used as an inertia (I_1, Fig. 2) which is coupled to the crankshaft (CS) by a rubber-ring. Hence, TVD is composed of an inner ring (hub) mounted on the crankshaft extremity, an intermediate viscoelastic rubber ring and an outer ring used as a poly-V pulley (Fig. 1). Generally, in simulation and for sake of simplification, the TVD dynamic properties – stiffness and damping – are chosen to be constant (Ewins et al., 2001). However, these properties depend on the operating temperature, the shear strain amplitude and the frequency to which the TVD is subjected since the rubber ring is made of a viscoelastic material (Lakes, 2009).

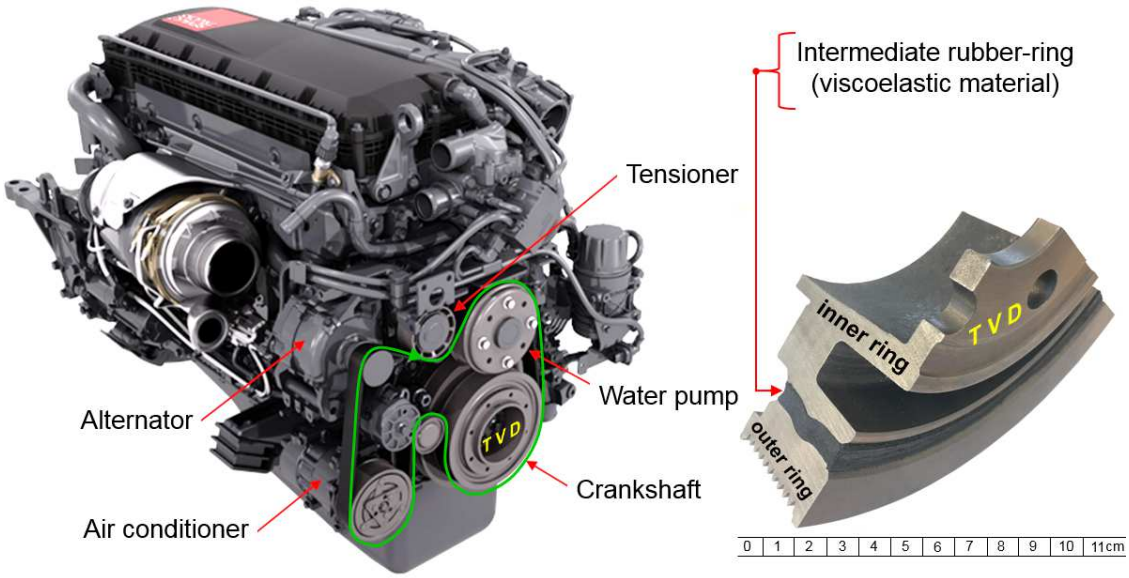

Figure 1. Serpentine poly-v belt of a FEAD with its TVD pulley.

In the literature, most of the works related to the account for rubber viscoelastic behavior in structural components (belt, pulley, dampers) of FEAD are about the impact of the poly-V belt viscoelasticity on its different vibration modes (Zhang and Zu, 1998; Marynowski, 2002; Marynowski and Kapitaniak, 2007; Chen and Ding, 2010; Ding and Chen, 2011). The viscoelasticity of the rubber layer embedded within the vibration dampers such as the TVD has rarely been explored. Recently, Bhatti (2012) indirectly compared viscoelastic dampers with Magnetorheological dampers. Also, the TVD behavior was investigated by Jauregui (1996) through a case study of a complicated model. A particularity of these studies is that they consider rheological models such as Maxwell (Bhatti and Varum, 2012), Kelvin (Jauregui et al., 1996; Kelly, 1962), etc. Such rheological models significantly increase the complexity of the differential equations of motion which are usually solved using complex numerical schemes.

Some other authors analyzed the dynamic characteristics of the stiffness and the damping from an experimental point of view (Kinoshita, 1989, and Wakabayashi, 1995). However, in the Wakabayashi's work, the results were fitted to a specific engine case. Recently, Manin et al. (2013) proposed a methodology to easily characterize the pulley torsional vibration damper.

The objectives of this paper are: (1) to propose a methodology based on the master curves of the TVD elastomeric layer, (2) then to simply and directly consider the viscoelastic properties of the constituting rubber-ring in the damper's equation of motion; (3) to highlight the influence of taking into consideration the viscoelastic properties of the elastomer when computing the TVD dynamic response; (4) to evaluate the coefficients of the equation of motion, stiffness and damping, as a function of the operating conditions.

This research aims at accurately calculating the viscoelastic TVD response in order to provide a realistic representation of the system dynamics, which is in accordance with Jauregui (1996)'s work and conclusions.

2 Torsional Vibration Damper modelling

2.1 Torsional damper dynamics

The torsional vibration damper can be modeled by a one degree-of-freedom (DOF) mass-spring-damper system (Blanc, 2000), it is also similar to the one DOF base excited vibrating system (Jazar, 2013), however in this case, the single DOF is the rotation around z-axis as shown in Fig. 2.

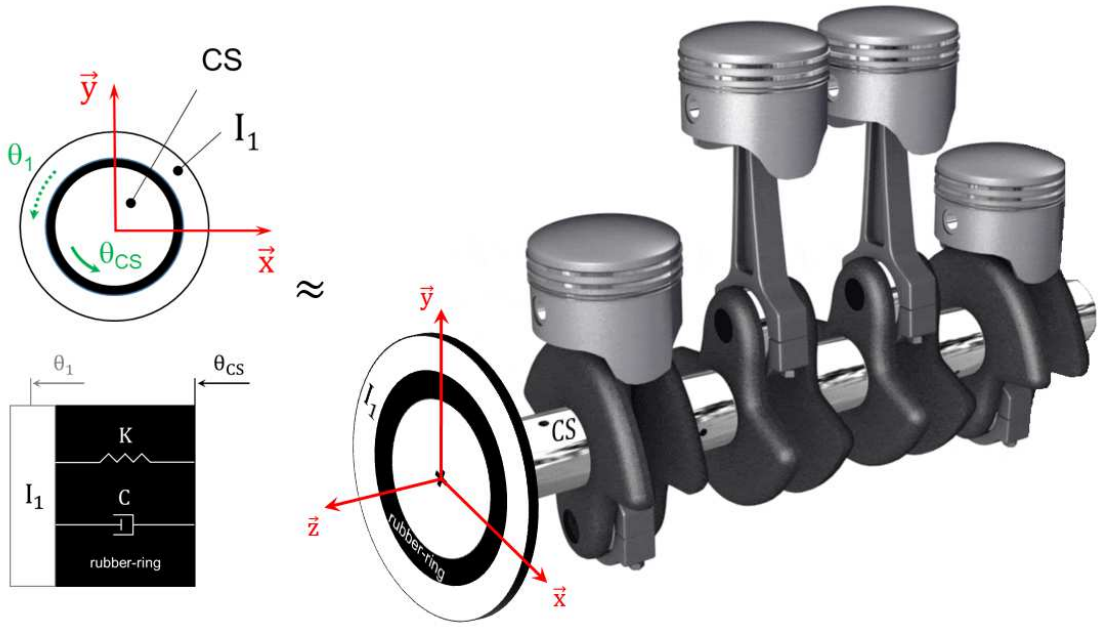

Figure 2. Torsional vibration damper and its schematic diagrams.

Assuming the engine at idling, the driving torque fluctuation usually contains 2 harmonics $(\omega, 2\omega)$. However, in this paper, only the prevailing harmonic (ω) and its amplitude (θ_{amp}) generally represented as $\theta_{CS} = \theta_{amp} \sin(\omega\, t)$ is considered to represent the acyclism on the crankshaft (θ_{CS}, Fig. 2). The difference between the torque experienced by the TVD outer-ring and the driving torque imposed by the crankshaft results in an angular lag of θ_1 with respect to the excitation θ_{CS}, and is due to the viscoelastic properties of the TVD intermediate rubber-ring.

To evaluate the impact of considering the intermediate rubber-ring temperature and frequency dependent viscoelastic properties leading to varying TVD stiffness K and viscous damping C coefficients, one considers the equation of motion of the system shown in Fig. 2, (Eq. 1):

$$I_1 \ddot{\theta}_1 + C \dot{\theta}_1 + K \theta_1 = C \theta_{amp} \omega \cos(\omega t) + K \theta_{amp} \sin(\omega t) \quad (1)$$

Where I_1 is the outer-ring inertia, angle θ_1 is the DOF considered, θ_{amp} and ω are, respectively, the amplitude and the excitation pulsation of the fluctuations (engine acyclism).

The steady-state response of θ_1 has an amplitude and phase as detailed in Eq. (2) (Jazar, 2013). This represents the Frequency Response Function (FRF) of one DOF base excited vibrating system with the frequency ratio r, natural frequency ω_n and damping ratio ξ as in Eq. (3).

$$\text{FRF}: \left\{ \frac{\theta_1}{\theta_{CS}} = \frac{\sqrt{1 + (2\,\xi\,r)^2}}{\sqrt{(1 - r^2)^2 + (2\,\xi\,r)^2}} \;\middle|\; \varphi_{\theta_1} = \tan^{-1}\left(\frac{2\,\xi\,r^3}{1 - r^2 + (2\,\xi\,r)^2}\right) \right\} \quad (2)$$

$$r = \frac{\omega}{\omega_n} \qquad \omega_n = \sqrt{\frac{K}{I_1}} \qquad \xi = \frac{C}{2\sqrt{K\,I_1}} \quad (3)$$

The equations (2) and (3) are considered because they are adapted from a classical formulation in the frequency-domain, which is consistent with the TVD elastomer DMA characterization presented in 3.1.

2.2 TVD rubber-ring viscoelastic model

The TVD intermediate ring is made of rubber which can be described as a viscoelastic material. A complex modulus E^* is usually defined to describe its response to a small strain oscillatory loading (Eq. 4).

$$E^* = E' + i\,E'' = f(T_{exp}, f_{exp}, \varepsilon_{exp}) \quad (4)$$

The real part of E^*, the storage modulus E' relates to the elastic behavior of the rubber, it defines the capacity to store energy upon deformation. The imaginary part of E^*, the loss modulus E'' defines the energy dissipative ability of the material. For the problem considered, the rubber-ring shall permit dampening the crankshaft torque fluctuations.
The complex modulus E^* is determined via DMA characterization and, for polymers, is known to vary as a function of the temperature T_{exp}, , the loading frequency f_{exp} and the dynamic strain ε_{exp} experienced by the rubber. Hence, the TVD intermediate ring material properties shall be determined in accordance with the engine-range of operating conditions (speed, temperature). Interestingly, for the material considered, the thermo-simplicity principle can be used (Silva et al., 2018) to predict the viscoelastic behavior of the rubber-ring at a given temperature T_{ref} (Fig. 5), i.e. the temperature in the engine room over a broad range of frequencies, which couldn't be assessed by DMA measurements otherwise. Practically, the DMA response curves measured for different temperatures and a limited frequency domain are horizontally shifted to form a unique/master curve (the vertical shift related to thermal expansion is often neglected). To a given temperature corresponds a shift factor a_T (Fig. 5, left). As a result, a master curve is constructed (Fig. 5, right). It will be

further fitted (Tab.2) in order to be used in the TVD viscoelastic model as explained in the next paragraphs.

2.3 Viscoelastic torsional damper model

When the viscoelasticity of the TVD rubber-ring is considered the equation of motion Eq.(1) becomes Eq.(5) with stiffness K_{var} and damping C_{var} which both depend on the temperature, the frequency and the dynamic strain similarly to the complex modulus E^* in Eq. (4).

$$I_1 \ddot{\theta}_1 + C_{var}\, \dot{\theta}_1 + K_{var}\, \theta_1 = C_{var}\, \theta_{amp}\, \omega \cos(\omega t) + K_{var}\, \theta_{amp} \sin(\omega t) \qquad (5)$$

Indeed, K_{var} and C_{var} are calculated from E^*. Let us examine the dependency of these terms on E^* and point out the way to determine them. The torsional stiffness K of the torsional vibration damper (TVD) in Figs. 1 and 3 can be estimated by Eq. (6) which was demonstrated by Blanc (2000).

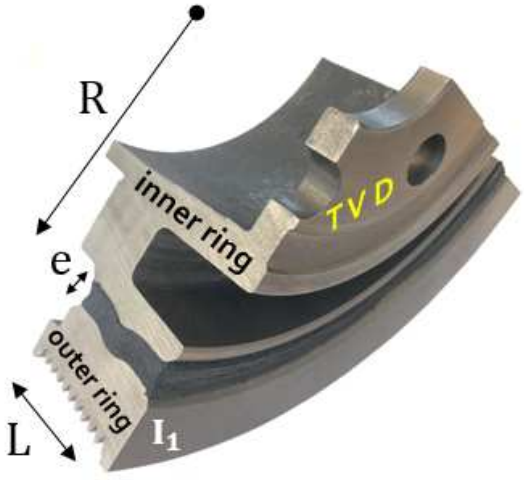

Figure 3. Geometrical parameters used to calculate the stiffness of the TVD.

$$K = \frac{2\,\pi\, R^3 L\; G'}{e} \qquad (6)$$

Where R, L, e are respectively the rubber-ring radius, width and thickness. The rubber-ring is assumed to be a homogeneous and isotropic material of shear modulus G'. Thus, Eq. (7) is valid for calculating G' from E' obtained via DMA with the Poisson ratio of the rubber $\nu \approx 1/2$.

$$G' = \frac{E'}{2\,(1+\nu)} \qquad (7)$$

Replacing G' by Eq. (7) in Eq. (6) the stiffness K_{var} can be calculated by Eq. (8).

$$K_{var} = \frac{\pi R^3 L}{e\,(1+\nu)}\,E' \tag{8}$$

As E' in Eq. (4), K_{var} varies as a function of the temperature T_{exp}, the frequency f_{exp} and the strain ε_{exp} experienced by the TVD rubber-ring. The viscous damping coefficient C can be calculated using the third term of Eq. (3) where the only unknown is the damping ratio ξ (Eq. (9)).

$$C = 2\sqrt{K\,I_1}\,\xi \tag{9}$$

Moreover, according to several authors (Piersol and Paez, 2010; Hujare and Sahasrabudhe, 2014) the structural loss factor η can be approximated as twice the damping ratio ξ, i.e. $\eta = 2\xi$ at resonance (Thomas and Laville, 2007) and $\eta = E''/E'$ for viscoelastic materials (rubber-ring) leading to Eq. (10).

$$C_{var} = \sqrt{K_{var}\,I_1}\,\frac{E''}{E'} \tag{10}$$

Similarly, C_{var} depends on the temperature T_{exp}, , the frequency f_{exp} and the strain ε_{exp} experienced by the TVD rubber-ring.

In the next paragraphs, the differences between Eqs. (1) and (5) are evaluated thanks to the TVD response (FRFs) for several operating conditions (temperature, frequency). The differences between the constant (K, C) and varying (K_{var}, C_{var}) stiffness and damping are also discussed.

3 Results

Results are presented for the TVD with the inertia and geometric parameters as detailed in Tab. (1). This is the crankshaft TVD used in the FEAD of a six-cylinder truck engine (Fig.1).

Table 1. Inertia and geometric parameters of the TVD considered.

I_1 (Kg mm^2)	R (mm)	L (mm)	e (mm)
31344.2	90	35	7

3.1 Dynamic Mechanical Analysis

The two components of the viscoelastic complex modulus E^*, namely the storage E' and loss E'' moduli, are used in Eqs. (7), (8) and (9) and thus need to be determined. To do so, Dynamic Mechanical Analysis measurements in tensile mode are performed on samples cut out of the TVD rubber-ring (Fig. 4).

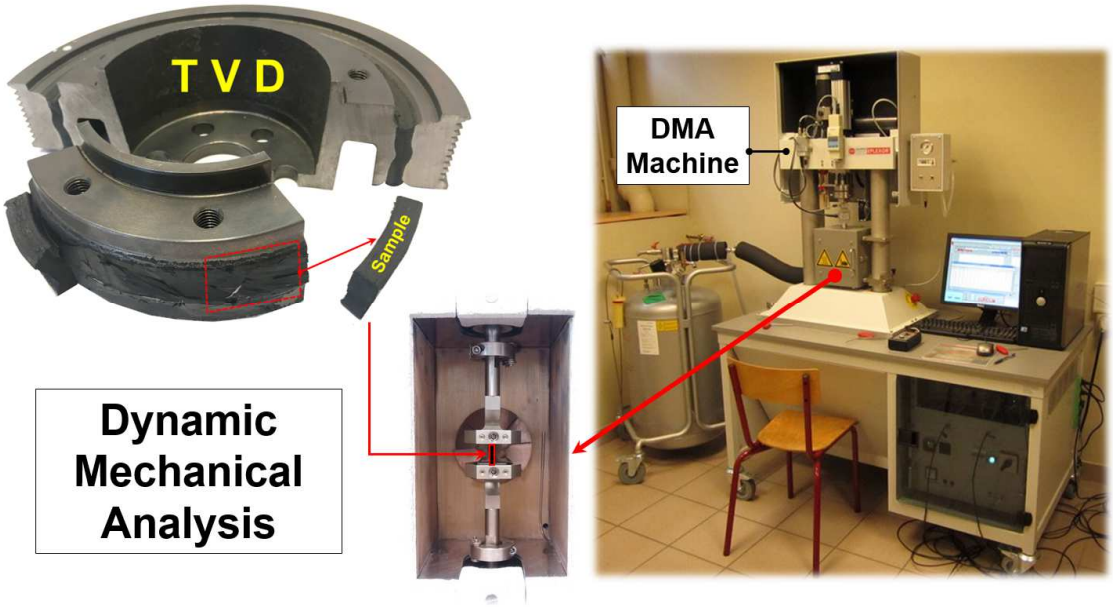

Figure 4. Experimental setup, principle and rubber-ring samples for the DMA tests.

More precisely, a forced periodic strain profile is imposed and the associated force is recorded. It is worth noting that the phase shift between the two time signals (strain and force) evidences the viscoelastic behavior of the tested sample. Furthermore, in order to explore the time temperature dependence, several frequencies and temperatures are considered. Finally, providing thermoreological simplicity of the material, the associated master curves can be determined for a given temperature of interest (the engine operating temperature).

In this work, three different frequencies (0.2, 2, 20Hz) and testing temperatures ranging from -10 to 120°C, were considered as evidenced in Fig. 5 (left). The resulting master curve at $T_{ref} = 20°C$ is plotted in Fig. 5(right), it permits predicting the mechanical behavior of the TVD rubber-ring at 20°C over a large frenquency range that can not be experimentally measured. In this study, master curves were obtained and fitted (Tab. (2)) for the engine operating temperatures of $20, 40, 60, 80$ and $100°C$.

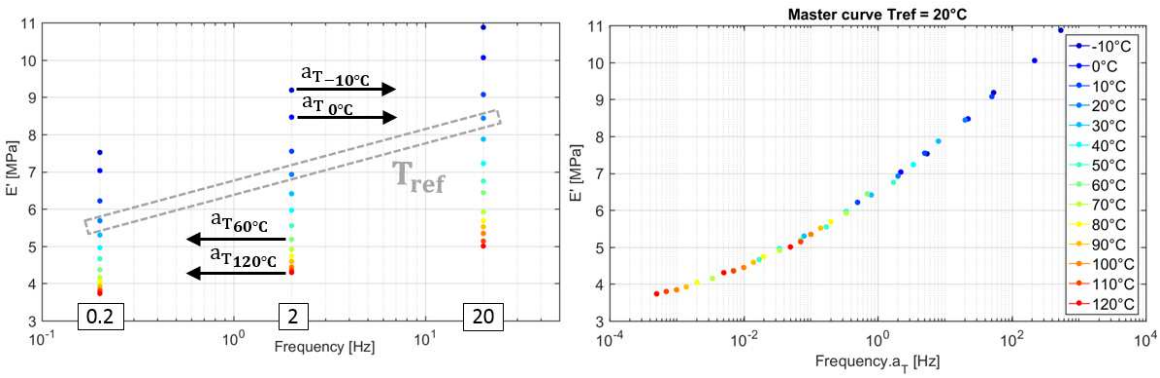

Figure 5. TVD rubber-ring DMA data (left) and correspondent master curve (right).

Table 2. Empirical equations describing the TVD rubber-ring moduli as $F(T_{ref}, f_{req}, \varepsilon = 0.002)$

T_{ref} (°C)	Storage $\dot{E}$ (MPa)	Loss modulus $E^{"}$ (MPa)
20	$6.55\ f_{req}^{\ 0.0814}$	$5.79\ f_{req}^{\ 0.0156} - 4.81$
40	$5.68\ f_{req}^{\ 0.0815}$	$5.41\ f_{req}^{\ 0.0163} - 4.58$
60	$5.02\ f_{req}^{\ 0.0820}$	$6.17\ f_{req}^{\ 0.0141} - 5.47$
80	$4.49\ f_{req}^{\ 0.0808}$	$6.07\ f_{req}^{\ 0.0139} - 5.49$
100	$4.27\ f_{req}^{\ 0.0835}$	$6.34\ f_{req}^{\ 0.0137} - 5.81$

3.2 Simulations

Table (3) gives data on stiffness and damping for the TVD which dimensions are given in Tab. (1). Both constant values K and C are used to simulate the constant FRF (dashed curves in Figs. 6 and 7) resulting in the resonance frequency of 216.5 Hz and damping ratio of 0.075 (Tab. (3)).

Table 3. TVD constant characteristics at $T_{exp} = 60°C$ used to determine the FRF

K (N m/rad)	C (N m s/rad)	Resonance (Hz)	Damping ratio ξ
58000	6.4	216.5	0.075

The TVD geometric parameters from Tab. (1) with its rubber-ring material properties (stiffness, damping) calculated from DMA characterization (Eqs. (8) and (10)) are then used in Eqs. (2) and (3) for several operating conditions of the torsional vibration damper producing the FRF plotted in Figs. (6), (7), (8) and (9).

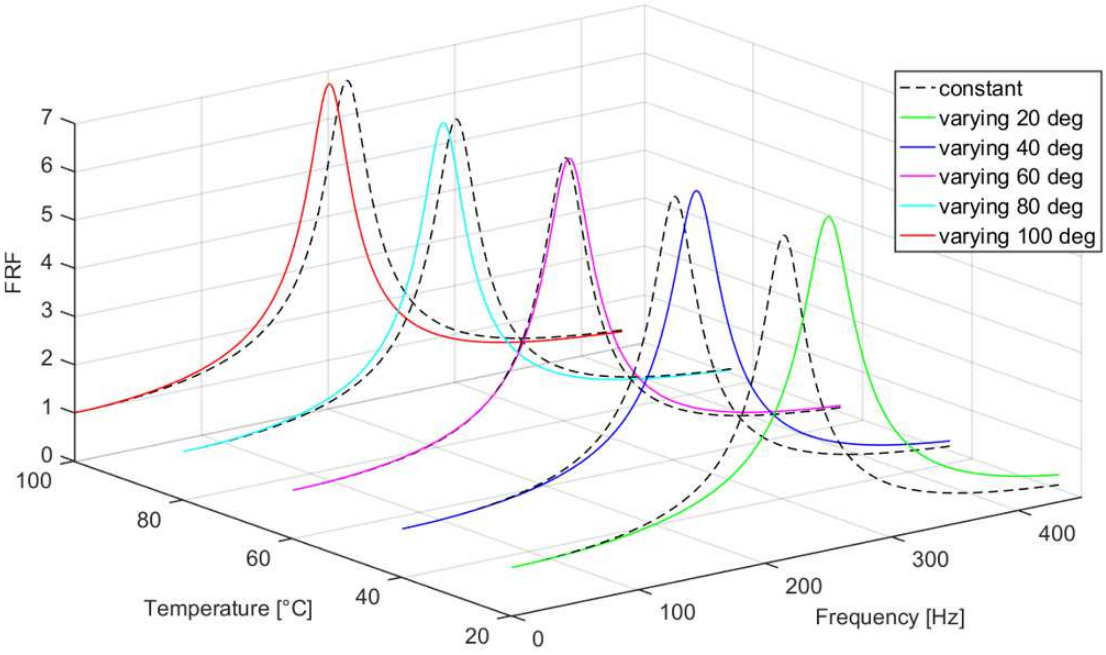

Figure 6. TVD amplitude, frequency response for several temperatures.

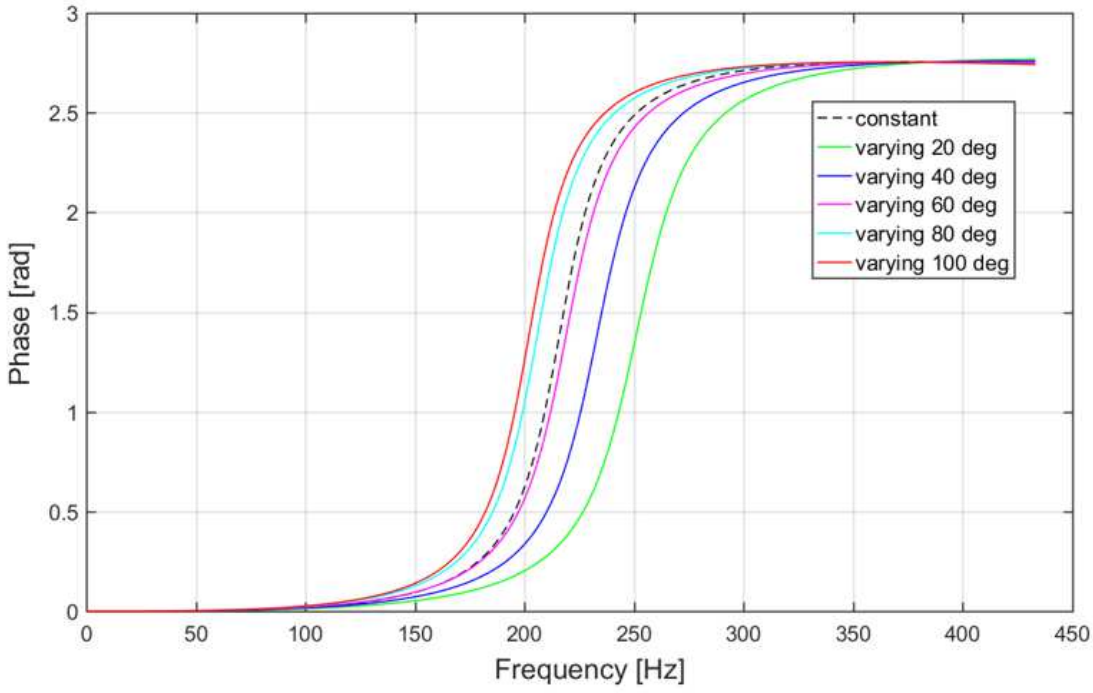

Figure 7. TVD phase, frequency response for several temperatures.

The differences between the FRFs in the Figs. 6 and 7 are proportional to the rubber-ring stiffness and damping variations in the Figs. 8 and 9 since the FRFs are generated using K_{var} and C_{var} in Eqs. (2) and (3). Thus, both the FRFs and the rubber-ring properties from

DMA vary with the TVD operating conditions (temperature, frequency) and the empirical equations in Tab. (2). In Fig. 6 when the TVD working temperature is changed, e.g. from $T_{exp} = 60°C$ to $80°C$, the maximum amplitude (peak) value of its FRF slightly changes (Fig. 10), which means that it changes by a few percent with a maximum of 3.3% at $T_{exp} = 20°C$ when compared to the constant case in Tab. (3) ($T_{exp} = 60°C$).

Assuming constant values for K and C ($FRF_{constant}$ in Fig. 6) with the same temperature ($T_{exp} = 60°C$) seems to be good approximations of the realistic K_{var} and C_{var} ($FRF_{60\ deg}$ in Fig. 6) with a maximum relative error of around 12.3 % (Fig. 11). However, throughout the engine range of operation, f_{exp} from 0Hz (engine at rest) to 2 times the TVD resonant frequency ($\sim$430Hz) in Fig. 11, the relative error increases substantially when the temperature is changed. For example, comparing the $FRF_{20\ deg}$ obtained at $T_{exp} = 20°C$ (K_{var} and C_{var} as in Eqs. (8, 10)) and $FRF_{constant}$ (K and C as in Tab. (3)) at $T_{exp} = 60°C$ the relative error $\left(FRF_{20\ deg} - FRF_{constant}\right)/FRF_{20\ deg}$ between these responses can reach around one hundred percent, see Fig. 11.

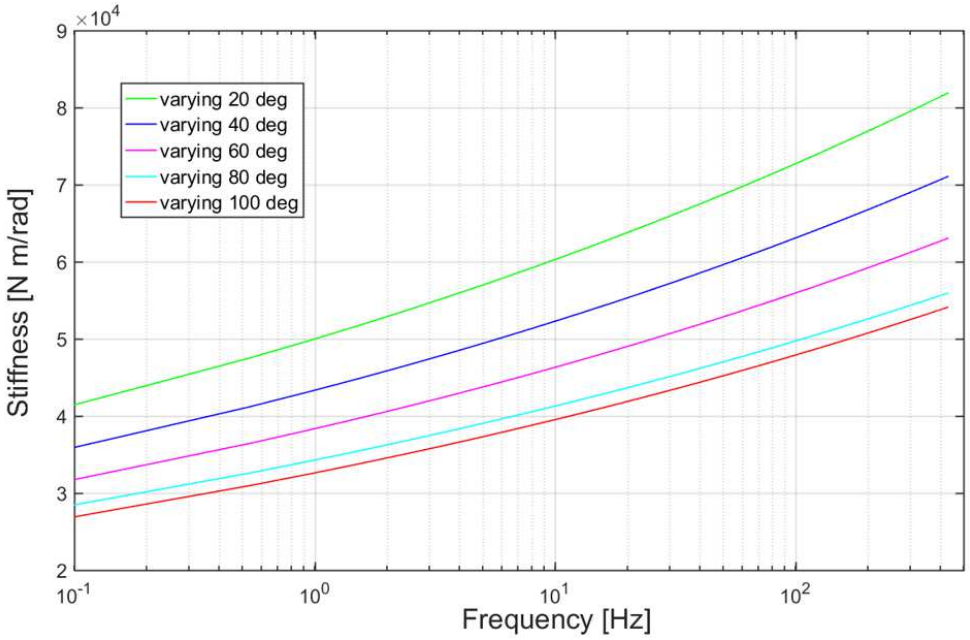

Figure 8. TVD rubber-ring stiffness K_{var} for several temperatures.

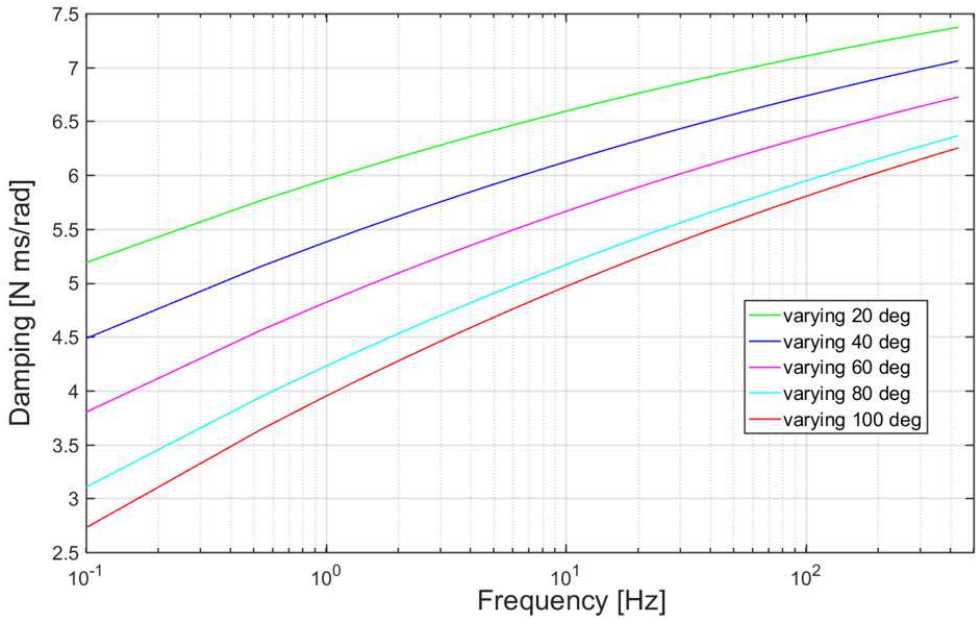

Figure 9. TVD rubber-ring damping C_{var} for several temperatures.

The range of the testing temperatures is chosen to be representative of the TVD working conditions, even in severe conditions of use, and the range of the excitation frequency is chosen to be equal in size to two times the TVD resonance frequency. Although, in practice, the resonance frequency corresponds to an operating point to be avoided, here, it permits analyzing clearly the change (viscoelasticity effects) in the frequency responses of the TVD thanks to the symmetry of the FRFs and shifting in relation to each other. The differences between the results obtained with constant and varying coefficients for several temperatures and the frequency domain equal to two times the TVD resonance frequency are also presented in Figs. (10) and (11).

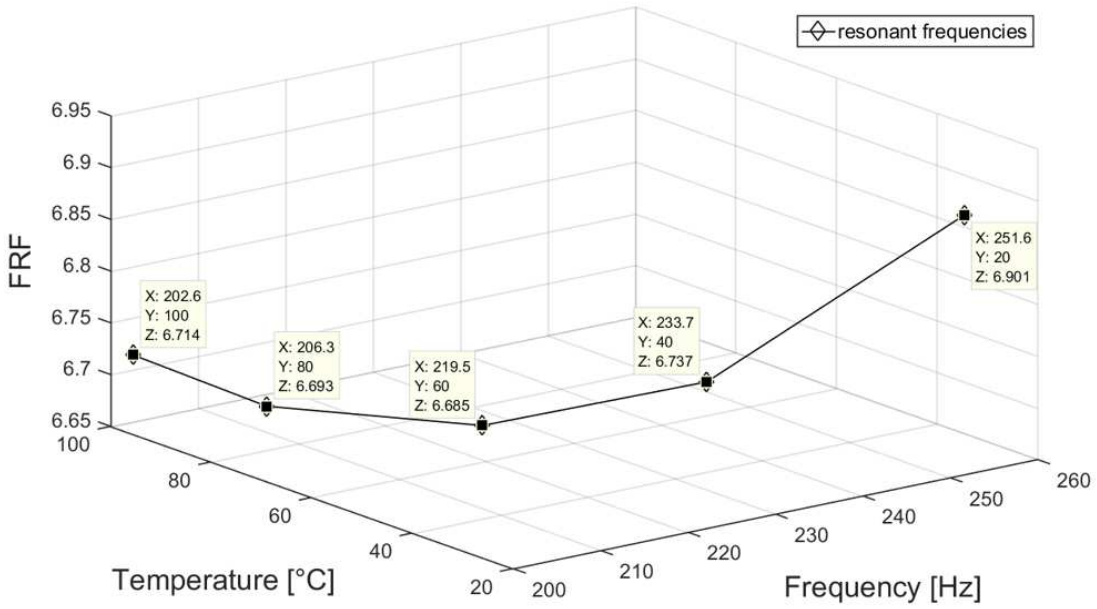

Figure 10. FRFs maximum peaks provided by K_{var} and C_{var}.

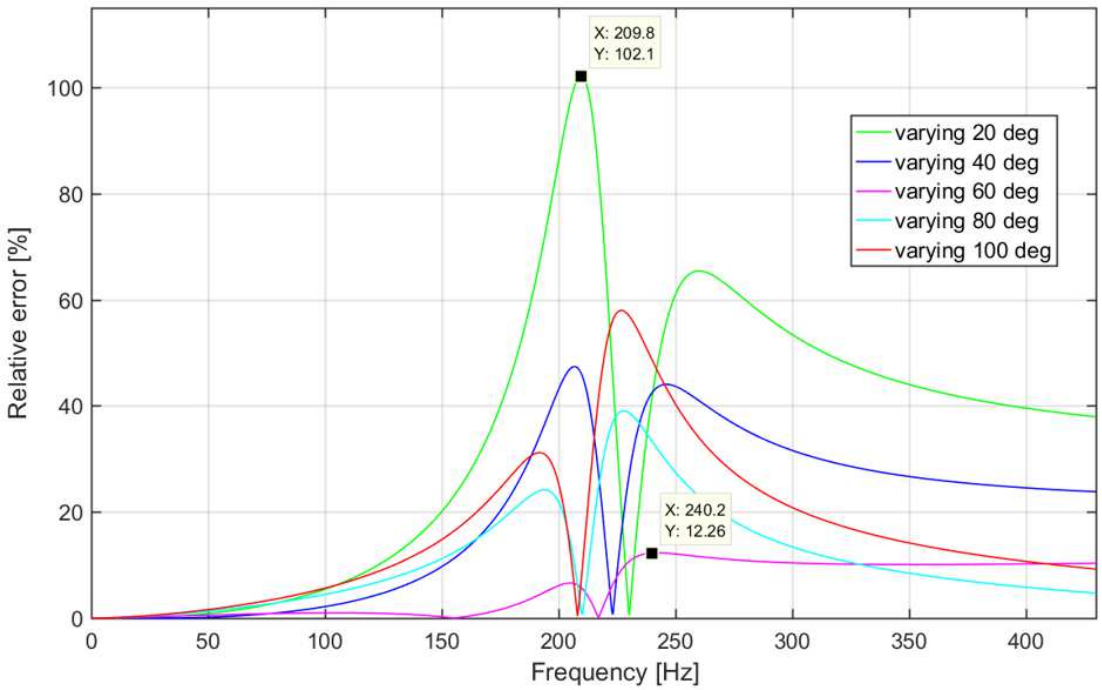

Figure 11. FRFs (relative) error made when K and C are used instead of K_{var} and C_{var}.

These results are summarized, discussed and verified experimentally in the next sections.

3.3 Experimental analysis

After generating numerical results for the case study (Tab. (1)) of the TVD in Fig. 1, one aimed at verifying experimentally the effectiveness of the TVD modeling as a single DOF system (Fig. 2) with varying stiffness and damping.

3.3.1 Set up description

An experimental setup has been designed to enable the measurment of the TVD frequency response when subjected to a torsional excitation under specific operating conditions, i. e. temperatures (Fig. 12). The temperature range was chosen to be representative of the TVD working conditions (25°C to 100°C) and according to the heating system capabilities. The range of the excitation frequency is chosen so that to be almost centred on the torsional resonance frequency (150 Hz – 350 Hz).

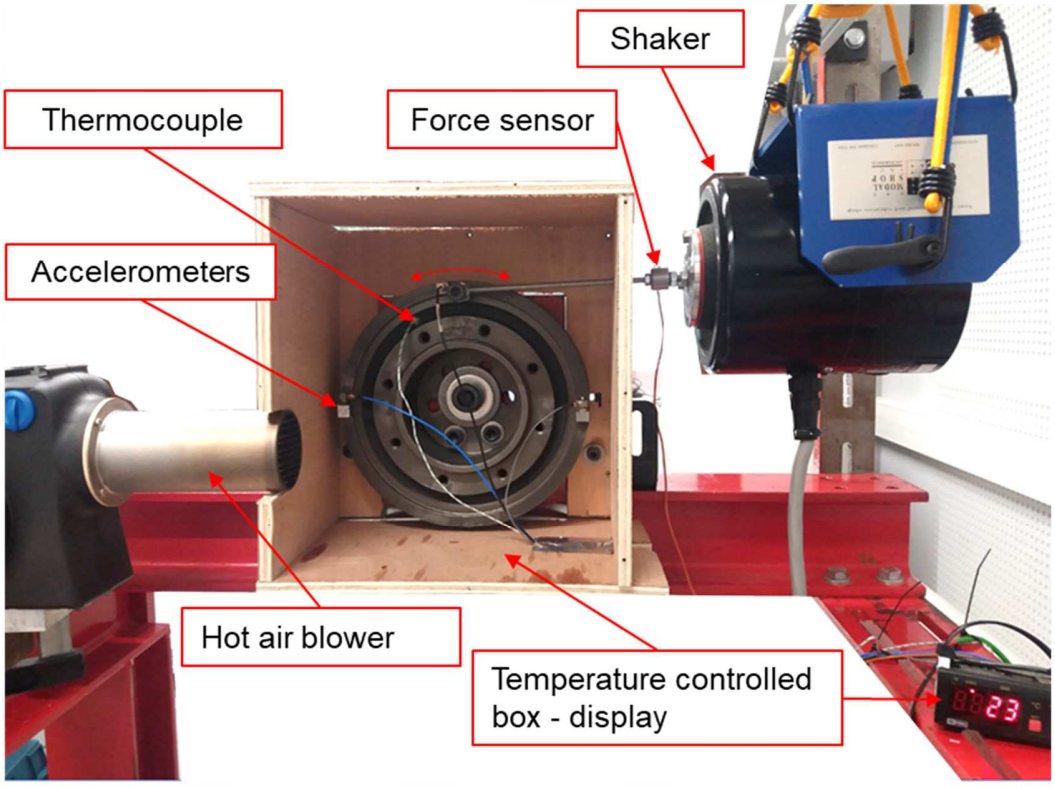

Figure 12. Experimental set-up used to test the TVD under specific operating conditions.

The principle of the experiment consists in exciting the TVD outer inertia with constant force of 5N applied by a shaker during a frequency sweep from 150Hz to 350 Hz. The response to this excitation is measured by accelerometers placed on the outer inertia so that to be sensitive to angular acceleration and therefore to permit analysing the torsional behavior. The hub of the TVD is bolted to a rigid frame, the outer-ring of the TVD is harmonically excited by a shaker through a push-rod system connecting the shaker head with the TVD outer ring. Since the excitation force is tangent to the pulley, it is also a torque/angular excitation for the outer ring with respect to its center. A hot air blower and a temperature controlled box (closed during the tests) are also used to increase the

temperature from the ambiant environment to the desired temperature. This testing temperature is measured by a thermocouple inserted in the TVD rubber-ring. Once the target temperature is reached, a stabilisation time of five minutes is applied before performing the frequency sweep. The input force is controlled and measured with a force sensor placed between the shaker head and the push-rod. The shaker and the excitation force are controlled by an M+P® control and acquisition system. Due to lack of time, the measurements have been done once for each temperature, therefore the variability of the experimental results are not discussed. The trends, consistency and agreement with simulations are analysed in next section.

3.3.2 Experimental results

The FRFs amplitudes and phases represented in Figs. 13 and 14 are obtained from the signals of the left accelerometer and the force sensor. As a result of the experiments, the stiffness and damping obtained experimentally through the half power bandwidth (3dB) method (Hujare and Sahasrabudhe, 2014) (Fig. 15 and Eq. (11)) show good agreement ($\leq$ 11% of error) with those obtained via simulations Eqs. (8) and (10) for the temperature of 60°C (Tab. (4)).

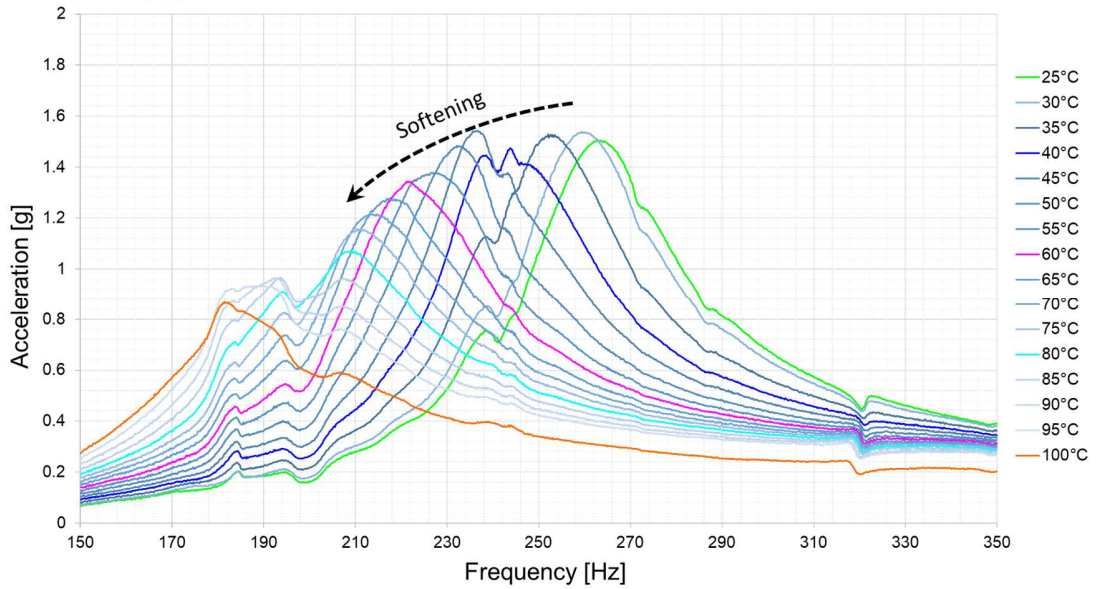

Figure 13. Experimental FRF (amplitude) of the TVD for several temperatures.

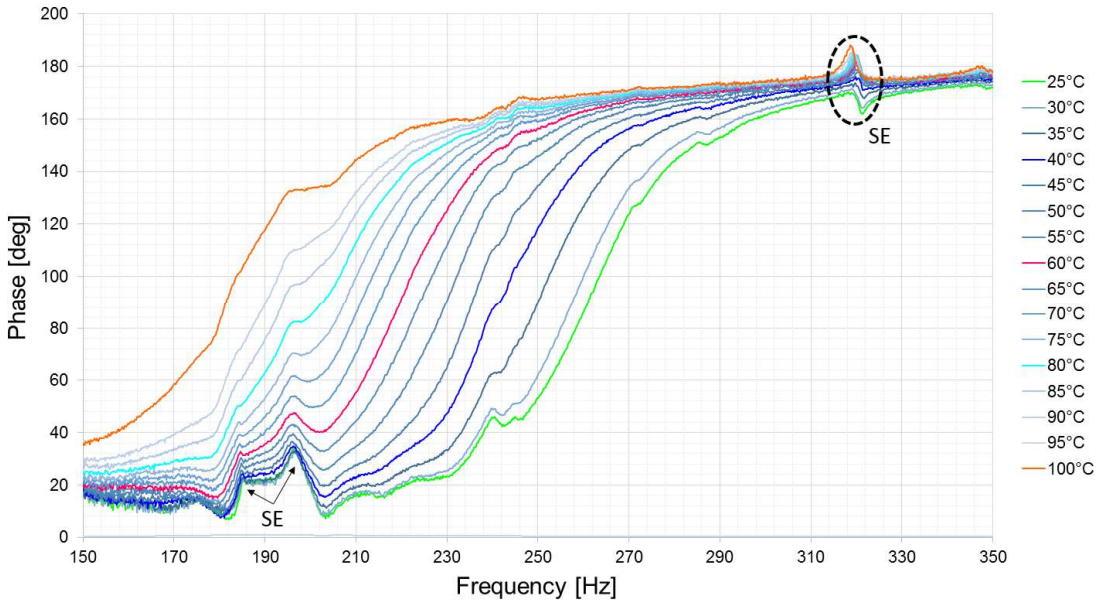

Figure 14. Experimental FRF (phase) of the TVD for several temperatures.

Table 4. Comparison between TVD stiffness and damping, simulated and measured at 60°C

	Stiffness [Nm/rad]	Damping [N ms/rad]	Resonance [Hz]	Damping ratio
Simulations	58000	6.4	216.5	0.075
Experiments	60526	5.8	221.2	0.067
Rel. error [%]	4.4	9.2	2.2	11.0

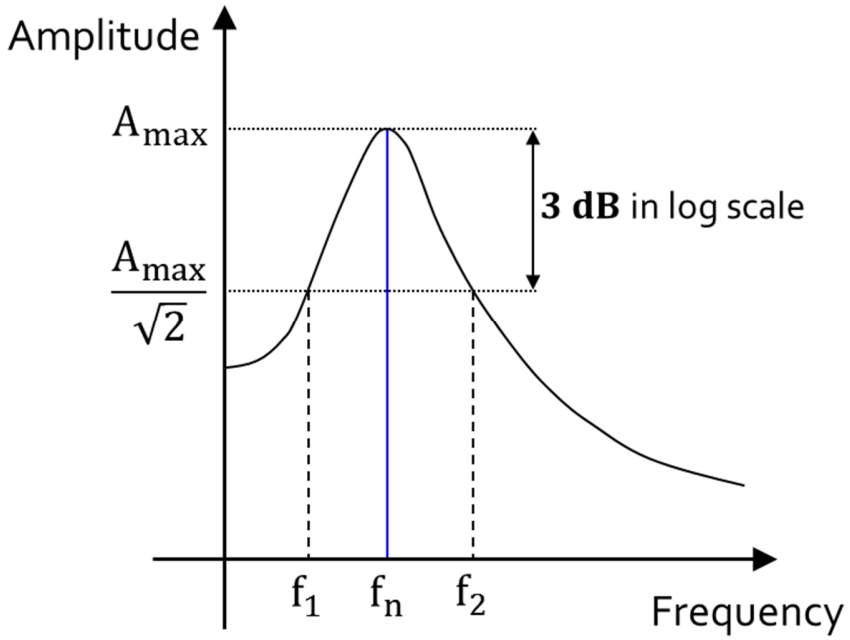

Figure 15. 3dB method applied to obtain the damping from the experimental FRFs.

$$\xi = \frac{f_2 - f_1}{2\, f_n} \tag{11}$$

The frequency responses (Figs. 13 and 14), obtained experimentally, confirm some interesting points observed in simulations: when the TVD working temperature is increased the resonance frequency is decreased and the FRFs are shifted to the left which coresponds to a softening behavior(Tab. (5)).

Table 5. Comparison of resonance peaks from simulations and experiments.

Temperature [°C]	Amplification [g]	Peak [Hz] experiments	Peak [Hz] simulations	Relative error [%]
25/20	*1.5*	*263.6*	251.6	4.7
40	1.5	243.8	233.7	4.2
60	1.3	221.2	219.5	0.8
80	1.1	209.2	206.3	1.4
100	0.6	206.9	202.6	2.1

It is observed that simulations results are in good agreement ($\leq$ 4.7% of error, Tab. (5)) with experimental results for several temperatures. The variability of the experimental results being not accessible since the tests were done once, the relative error has to be considered with some criticism even if it is satifactory. The small difference between the peaks obtained numerically and experimentally may be due to the 3dB method which introduces a constant error. However, the absolute value of the shifts when the temperature

is changed are equivalent validating experimentally the results predicted numerically. For temperatures up to 80°C the frequency response curves change shape and a secondary peak appears (Fig. 13). At 100°C the torsional resonance is observed experimentally for 206,9 Hz (0,6g) but the peak amplitude is smaller than that at 182 Hz (0,86g). The corresponding phase curve shows two inflections at these later frequencies (Fig. 14). This phenomenon may be due to the emergence of a structural vibration mode of the test apparatus that is no more negligible since the rubber ring becomes softer. This shows the limits of the experimental set up for high temperatures.

4 Discussion and Conclusions

In this paper, the TVD response is analyzed as a function of its operating conditions (temperature, frequency) because it is assumed here that the moduli in Eq. (4) and, consequently, the torsional stiffness K_{var} and damping C_{var} depend exclusively on the temperature and the frequency (Silva et al., 2018), i.e. no Payne effect. Thus, for the constant strain $\varepsilon_{exp} = 0.2\%$, different operating conditions lead to different responses as in Figs. 6 and 7.

An interesting point when considering the viscoelasticity of the TVD rubber-ring is the different resonant frequencies in Tab. (5) accordingly with the operating conditions. When the temperature is increased the TVD resonance peak is shifted to the left. This is because the stiffness K in Eq. (6) depends on G' which depends on E' (Eq. (7)). Thus, as the stiffness K is operating conditions dependent (Eq. (4)), the resonance frequency of the TVD calculated by the second term of Eq. (3) also depends on its operating conditions.

Finally, the comparisons between simulations and experiments show good agreement with small relative error (Tab. (5)). However, when the temperature is increased the FRFs are more dampened (smoothing, Fig. 13) and there are some side-effects (SE, Fig. 14). These may be due to the complex viscoelastic material behavior and due to the fact of not being able to impose a pure torsional mechanical excitation to the TVD experimentally. It means that there are also the response of other modes (directions) in the experimental FRFs.

Acknowledgement

The authors are very grateful to the Auvergne Rhone Alpes council, Volvo-Renault Trucks and the FEDER fund who supported this work.

References

[1] Bhatti AQ and Varum H (2012) Comparison between the visco-elastic dampers and magnetorheological dampers and study the effect of temperature on the damping properties. In: *15th World Conference on Earthquake Engineering*, Lisboa, Portugal, 24-28 September, pp. 8297-8305. New York: Curran Associates Inc. Proceedings.

[2] Blanc H (2000) Dynamique des rotors en torsion Etude des amortisseurs de torsion. *Techniques de l'Ingenieur*, Réf. : BM5124 V1

[3] Chen LQ and Ding H (2010) Steady-state transverse response in coupled planar vibration of axially moving viscoelastic beams. *ASME J. Vib. Acoust* 132 (1): 1-9. DOI: http://dx.doi.org/10.1115/1.4000468

[4] Ding H and Chen LQ (2011) Nonlinear models for transverse forced vibration of axially moving viscoelastic beams. *Shock and Vibration* 18: 281-287. DOI: 10.3233/SAV20100586

[5] Ewins D, Rao SS and Braun SS (2001) *Encyclopedia of Vibration*. Oxford: Academic Press, pp.165-174. DOI: http://dx.doi.org/lO. 1006/rwvb.2001

[6] Hujare PP and Sahasrabudhe AD (2014) Experimental investigation of damping performance of viscoelastic material using constrained layer damping treatment. *AMME Procedia Materials Science* 5:726-733. DOI: https://doi.org/10.1016/j.mspro.2014.07.321

[7] Jauregui JC, Becerril JA and Guzman AL (1996) Viscoelastic torsional damper model. In: *ASME Power Transmission and Gearing Conference*, New York, USA, pp. 777-780.

[8] Jazar RN (2013) Advanced Vibrations - A Modern Approach. In: Vibrations Fundamentals (Frequency Response) *Base Excitation*. New York: Springer, pp. 197-209. DOI: 10.1007/978-1-4614-4160-1

[9] Kelly JM (1962) *Moving load problems in the theory of viscoelasticity*. PhD Thesis, Stanford University, USA.

[10] Kinoshita M and Sakamoto T (1989) An experimental study of a torsional/bending damper pulley for an engine crankshaft. *SAE Technical Paper* 891127. DOI: https://doi.org/10.4271/891127

[11] Lakes RS (2009) *Viscoelastic Materials*. Cambridge: University Press.

[12] Manin L, Dufour R and Schultz S (2013) Pulley torsional vibration damper characterization. *Mechanics & Industry* AFM EDP Sciences 14:151-155. DOI: 10.1051/meca/2013057

[13] Marynowski K (2002) Non-Linear Dynamic Analysis of an Axially Moving Viscoelastic Beam. *J. Theor. Appl. Mech.* 2(2): 465-482.

[14] Marynowski K and Kapitaniak T (2007) Zener internal damping in modelling of axially moving viscoelastic beam with time-dependent tension. *Journal of Non-Linear Mechanics* 42 (1):118-131. DOI: https://doi.org/10.1016/j.ijnonlinmec.2006.09.006

[15] Piersol AG and Paez TL (2010) *Harris' Shock and Vibration Handbook*. New York: McGraw Hill

[16] Silva CAF, Manin L, Rinaldi RG, Remond D, Besnier E and Andrianoely M-A (2018) Modeling of power losses in poly-V belt transmissions: hysteresis phenomena (enhanced analysis). *Mech. Mach. Theory* 121: 373-397. DOI: https://doi.org/10.1016/j.mechmachtheory.2017.10.008

[17] Thomas M. and Laville F (2007) *Simulation des vibrations mécaniques*. Québec : Presses de l'Université du Québec

[18] Wakabayashi K, Honda Y, Kodama T and Shimoyamada K (1995) Torsional vibration damping of diesel engine with rubber damper pulley. *JSME International Journal* Series C 38(4): 670-678. DOI: https://doi.org/10.1299/jsmec1993.38.670

[19] Zhang J and Zu JW (1998) Non-linear vibrations of viscoelastic moving belts. *Journal of Sound and Vibration* 216: 93-105. DOI: https://doi.org/10.1006/jsvi.1998.1689